Non-invasive aging analysis of lithium-ion batteries in extreme cold temperatures

Adrian Soto, *Student Member, IEEE,* Alberto Berrueta, *Member, IEEE,* Ignacio Oficialdegui, Pablo Sanchis, *Senior Member, IEEE,* and Alfredo Ursúa, *Senior Member, IEEE.*

***Abstract*— This paper presents a non-invasive technical analysis of the degradation of four lithium-ion batteries (LIBs) used in extreme frigid weather. In contrast to other studies in which the batteries were tested in laboratory conditions, the LIBs studied in this paper were aged in a real application, more specifically in the WindSled project. In this project, an expedition was made using a zero-emission vehicle drawn by kites, covering more than 2500 kilometers on the East Antarctic Plateau. The study performed in this paper aims to quantify the degradation of the LIBs during the expedition. The results show a 5 % capacity fade, a 30 % increase in the internal resistance and no substantial increase in the impedance of the solid electrolyte interface (SEI). Moreover, no evidence of dendrite growth at the anode is inferred by the interpretation of the distribution of relaxation times (DRT), incremental capacity analysis (ICA) and differential voltage analysis (DV). Based on these results, it can be claimed that the LIBs used in the WindSled Project can successfully operate under –50 ºC. Furthermore, since non-invasive techniques were used to characterize the batteries, they can still be used in upcoming expeditions, with subsequent financial and environmental benefits.**

***Index Terms*—Battery, DRT, DV, EIS, energy storage, ICA, lithium-ion, temperature.**

I. Introduction

SINCE the industrial revolution in 1769, the atmospheric concentrations of CO_2 have increased relentlessly. Although industrial development has made it possible for people to achieve levels of cultural, scientific and social well-being that were completely unattainable a few centuries ago, there is an increasing need to replace the current energy model with one in which energy generation and storage are not dependent on fossil fuels. It is therefore normal to find research proposals to address this issue.

Over the last decade, lithium-ion batteries (LIBs) have been put forward as the best storage alternative for the transport sector as well as for grid support [1]–[4]. Despite its high efficiency, energy density and power density, this technology, which is based on electrochemical reactions with ion intercalation, still needs to overcome a number of challenges.

This work was supported in part by the Spanish State Research Agency (AEI) under Grant PID2019-111262RB-I00/AEI/10.13039/501100011033, in part by the European Union under the H2020 Project STARDUST under Grant 774094, and in part by the Public University of Navarre through the research project ReBMS PJUPNA1904 and a Ph.D. Scholarship.(*Corresponding author: A. Ursúa*).

The authors are with the Department of Electrical, Electronic and Communications Engineering, Institute of Smart Cities, Public University of Navarre, 31006, Pamplona, Spain (e-mail: adrian.soto@unavarra.es; alberto.berrueta@unavarra.es; pablo.sanchis@unavarra.es; alfredo.ursua@unavarra.es).

Ignacio Oficialdegui is with the WindSled project (email: ofiignacio@gmail.com)

From a technical point of view, the operation of LIBs at subzero temperatures is one of the most critical factors, for two reasons. Firstly, the power and energy capacities of LIBs are reduced [5]. Secondly, it leads to accelerated aging phenomena that can induce catastrophic battery failures [6].

The anode, which is usually made of graphite, is the battery component to limit low-temperature operation. With regard to battery charging particular attention should be paid to lithium plating. This process consists in the deposition of metallic lithium on the solid electrolyte interface (SEI) at the anode, leading to an irreversible capacity fade. Moreover, there is also an increase in impedance, since the remaining ions cannot migrate through the plated lithium. Furthermore, this can result in an internal short-circuit due to the dendrites built by the metallic lithium. The poorer performance of LIBs under low temperatures has been duly reported in the literature, measuring capacity reductions of 30% at 5ºC [7]. Considering the battery internal resistance, previous studies report increases of up to 15- fold at –20 ºC [8].

This paper makes an in-depth analysis of the performance of the LIBs used in the WindSled project, a scientific expedition carried out in East Antarctica, the coldest area on Earth. Due to the incipient environmental interest in Antarctica, the laboratory and personnel forming part of the expedition traveled in the sled shown in Fig. 1, drawn solely by kites. The electricity required for survival and for the scientific experiments was delivered by flexible PV panels installed on the sled. This electrical energy was stored in LIBs specially designed to withstand the extreme temperatures, close to –50 ºC, during the 52 days of the journey. The expedition succeeded in performing ten scientific experiments with high international impact [9].

The aim of this study is to report on the technical viability of LIBs as an electrical energy storage system in frigid weather conditions, providing in-depth characterizations of the batteries used and inferring the most critical aging phenomena suffered

Fig. 1. A picture of the WindSled taken during the expedition.

by these LIBs. The novelty of this contribution is related to the fact that the batteries were not aged in a laboratory under predefined conditions, but in a real-life expedition where the operation was not simply realistic, but actually real. On the one hand, this work provides a comprehensive overview of the current non-invasive techniques directed at identifying the internal changes taking place in LIBs. The physical changes occurring during the aging process cannot be inferred by simple electrical measurements such as capacity, which is insufficient to assess the reliability of re-using an LIB. Therefore, tests to infer the interior physical condition of the cells are required. On the other hand, the reasoning and interpretation of the results obtained were applied to a real scenario in which the operating conditions could trigger hazardous aging caused by dendrite growth. Therefore, this work could serve as a guideline for future investigation in which the feasibility of battery reuse needs to be demonstrated. The main advantage of this proposal is that the entire test methodology is non-invasive and so there is no damage to the cells during testing.

The remainder of this paper is organized as follows. Section II gives a brief description of the polar expedition, including the energy storage systems. Section III provides a compilation of the main characterization techniques for LIBs, as well as an analysis of their suitability for the analysis of sub-zero operation. Section IV presents the proposed experimental procedure and tests carried out on the LIBs. Section V analyzes the results, that show the effect of freezing weather on LIBs. Finally, Section VI summarizes the main results and presents the conclusions.

II. Expedition

A. Details of the expedition

The WindSled project has demonstrated the feasibility of conducting an expedition to Antarctica using only the sun and wind as power sources. The sled covered 2538 km in 52 days reaching a maximum altitude of 3768 m above sea level (Dome Fuji). This non-motorized vehicle departed from the Russian base of Novalazárevskaya on December 12th 2018 and returned on February 1st 2019, going beyond places such as the North American research base Plateau Station and Dome Fuji.

The WindSled comprises the three modules shown in Fig. 1, with a total length of 9 meters and width of 4 meters, carrying a total weight of up to 2 tons and with room for up to 6 crew members. The first is the locomotive module, which serves to control the kites and to serve as a scientific workshop. The second is the cargo module to store the scientific equipment, groceries and expedition materials. Furthermore, the cargo module is covered by 12 m^2 of flexible PV panels, used to charge the 4 LIBs studied in this paper. The final module corresponds to the living quarters.

B. The energy storage system

Lithium-ion batteries were used as the energy storage system for this expedition. The critical requirements for these LIBs are a high energy density and reliability at low temperatures (down to – 50 ºC). The batteries chosen for WindSled project were assembled by a 4S4P connection of 16 MP176065 xtd cells from Saft [10]. These cells use Lithium-Nickel-Cobalt-Aluminum Oxide (NCA) as the cathode material and a graphite-based anode. The cells have an operating range from –40º C to 85ºC. This extended range could be explained by an improvement in the electrolyte by means of additives or co-solvents with low melting points and low viscosity. Further information on the cell performance can be found in [11]. The cells have a rated voltage of 3.65 V and a rated capacity of 5.6 Ah, giving a battery voltage of 14.6 V and a capacity of 22.4 Ah. Each battery, including the BMS, weighs 2.7 kg, achieving an energy density of 120 Wh/kg.

Even though the battery cycling profile during the expedition was not as well characterized as in a laboratory experiment, the main operating characteristics of each battery are summarized below. Further information regarding the equipment consumption and describing the experiments conducted in the WindSled project is provided in [9].

- Battery 1 (E1): powers the AEMET weather station and is charged by a 90 W PV panel. Fully discharged several times.
- Battery 2 (E2): powers the ESA equipment and is charged by a 75 W PV panel. Kept at high *SOC* for the entire expedition.
- Battery 3 (E3): powers the MICROAIRPOLAR equipment and is charged by a 75 W PV panel. Fully discharged several times but to a lesser extent than E1.
- Battery 4 (E4): unused. It was short-circuited during the first day of the expedition at a *SOC* of 80 % due to a human error. The battery was not damaged, but the internal protection fuse rendered it unusable.

III. Characterization techniques for LIBs

The correct characterization of an LIB provides decisive information about battery functionality. The main electrical parameters that characterize a battery are the capacity, internal resistance, open circuit voltage (V_{OC}) and state of charge (*SOC)* relationship, and self-discharge. Furthermore, through non-invasive characterization techniques and their subsequent analysis and interpretation, the aging mechanism can be glimpsed. In this section, a brief explanation of each parameter is given, along with a description of the most common experimental tests used for quantification purposes.

A. Capacity

Capacity measurement should be performed under controlled temperature conditions, usually at 25 ºC [12], and with standardized current profiles. The current is usually kept below C/3 for correct capacity measurement, in order to avoid self-heating processes [13].

A full charge – discharge cycle not only permits capacity measurement, but also an estimation of the current state of the electrodes [12]. For this purpose, the incremental capacity analysis (ICA) $dQ/dV = f(V)$, and differential voltage analysis (DV) $dV/dQ = f(Q)$ can be performed. Given that the V_{OC} of a cell depends on the balance between the positive and negative electrodes, it is affected by the aging phenomena [12]. As highlighted in previous studies [14], currents under C/2 are suitable

for ICA/DV studies since the major peaks can be clearly identified with this current.

Typically, two major peaks can be observed in the ICA for graphite+NCA cells. The peak occurring at a lower voltage is commonly used as an indicator of the underlying reactions on the anode, while the sequential phase transition process in the cathode dominates the higher voltage peak [14]–[16]. In a similar way, the DV can be used to infer the loss of lithium inventory (LLI) and/or the loss of active material (LAM). The DV curve can be split into three regions, Q_a, Q_b and Q_c. A reduction in Q_a and/or Q_b indicates a loss of active material on the anode [14], [17]. In contrast, a reduction in Q_c is related to the LLI [18], [19].

LLI is commonly associated with aging phenomena that consume Li ions from parasitic reactions such as lithium plating and/or inactive species precipitation [12], [19], [20]. On the other hand, mechanisms affecting the amount of active materials, such as dissolution and/or grain isolation are related to LAM [12], [19]. Many studies have reported LLI to be the main cause of capacity loss [20], [21].The aging mechanism known as lithium plating, specifically at low temperatures, can lead to dendrite growth and accelerate SEI formation [19]. Some authors draw a distinction between LLI and lithium plating. The effect of lithium plating can be seen in an ICA curve as the emergence of a new low amplitude and high voltage peak [20], [22], [23]. This peak can be used as a lithium plating indicator.

B. Impedance

The battery impedance can be measured by exciting the LIB with a current pulse or with a sinusoidal signal. Related to the real part of the impedance (resistance) two relevant values are usually provided: R_{DC} is the battery resistance for low-frequency operation and R_{AC} is the resistance at high-frequency operation.

The most common technique for the measurement of R_{DC} consists in the application of a current step (ΔI) to a relaxed battery. With the measurement of the voltage response (ΔV), R_{DC} can be calculated by means of Ohm's law, as shown in (1). Due to the simplicity of this method, LIBs are modeled with a low computational cost, which is desirable in many electrical engineering applications [24], [25].

$$R_{DC} = \frac{\Delta V}{\Delta I}. \tag{1}$$

A more comprehensive measurement of the battery impedance can be addressed through an electrochemical impedance spectroscopy (EIS). This technique provides information about most material properties, interfacial phenomena and electrochemical reactions [26]. In Fig. 2, a graphical representation of a typical EIS of a LIB is presented by a Nyquist plot. The intersection of the impedance plot with the real axis corresponds to the internal ohmic resistance, which includes the ionic conductivity of the electrolyte and the electronic conductivity of the electrodes, current collectors and electrical contacts [27].

Low frequencies of less than 0.5 Hz are dominated by diffusion. The ion migration inside the electrodes and electrolyte is driven by law of diffusion and by the concentration gradient [28].

In the mid-frequency range of an EIS, either one or two arcs can be seen depending on the state of the battery. The cell characteristics that determine the shape and size of the arcs are the charge transfer resistance, the double-layer capacitance of the anode, the double-layer capacitance of the cathode, and the resistance of the SEI layer [27]. This mid-frequency impedance is highly dependent on the battery *SOC*, since the ion concentration and the lattice structure of the electrodes depend on the *SOC*. The NCA cathode charge transfer is the dominant process of the arc at low *SOC*s [29], whereas at high *SOC*s, the critical component is the graphite anode [30]. The interpretation of this mid-frequency range is the most challenging data processing task, given that various electrochemical effects have similar time constants [28]. Over the las few years, the distribution of relaxation times (DRT) method is gaining popularity [31], [32]. This analysis is based on the probability of a process occurring within a specified time constant. The measured impedance data in the frequency domain are deconvoluted to fit the following expression

$$Z(f) = R_{ohm} + \int_0^\infty \frac{g(\tau)}{1+j2\pi f\tau} d\tau \tag{2}$$

where R_{ohm} is the ohmic resistance, $g(\tau)$ is the distribution of relaxation times, j the imaginary unit, f the frequency and τ the time constant. Note that this method assumes an impedance model built by infinite R||C branches connected in series, the impedance of each branch can be expressed in the frequency domain as:

$$Z(f) = \frac{R}{1+j2\pi\, f\, R\, C}. \tag{3}$$

The impedance data is generally acquired in a logarithmic scale. Thus, (2) can be rewritten as

$$Z(f) = R_{ohm} + \int_{-\infty}^{\infty} \frac{\gamma(ln\tau)}{1+j2\pi f\tau} dln\tau \tag{4}$$

being

$$\gamma(\ln\tau) = \tau g(\tau). \tag{5}$$

Relevant information about the correlation between the DRT and the underlying physical phenomena has been published in the literature. Firstly, the SEI resistance has been proven to have no significant dependence on *SOC* for *SOC*s greater than 10% [33]–[35]. Typical values of the SEI characteristic frequency are 16 – 160 Hz [33], 36 – 76 Hz [34], or 28 – 50 Hz [35].

At low *SOC*s, the charge transfer at the cathode becomes the

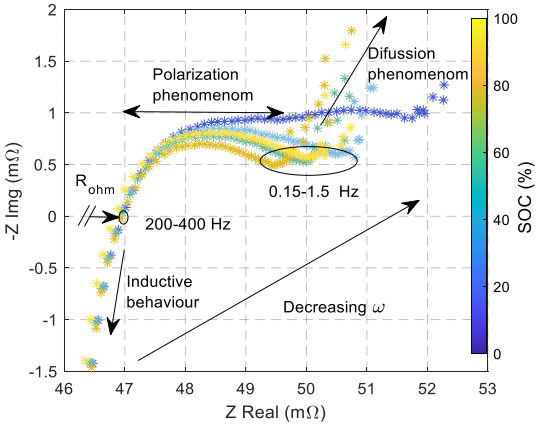

Fig. 2. Typical EIS of a LIB at various *SOC* levels.

dominant process. In a recent publication [30] analyzing an NCA cathode and graphite anode cell, like the ones studied in this paper, the characteristic frequency of the charge transfer at the cathode varies from 0.4 Hz to 2 Hz depending on *SOC*. At the same time, a frequency of about 5 Hz was identified with the charge transfer phenomenon in the anode.

C. Self-discharge

Self-discharge of an LIB is the reversible loss of charge, which results in a voltage decay throughout the storage time. The three main reaction mechanisms are the absorption of electrons and ions at the SEI layer, the reversible reduction of carbon dioxide to oxalate, and the side reactions between the anode and cathode [36], [37].

The most widely-used method to measure the self-discharge of a battery is based on measuring the voltage decay throughout the storage time (dV_{OC}/dt) [36]. The reversible capacity loss ΔC is obtained by means of (6).

$$\Delta C = [SOC(V_{OC_1}) - SOC(V_{OC_2})] \cdot \frac{C}{100} \quad (6)$$

where V_{OC1} is the open circuit voltage measured at time 1, V_{OC2} is the open circuit voltage measured after a given storage time (at time 2), and C is the cell capacity.

Self-discharge presents different characteristics in the short and long term. In the short term (less than three weeks) the voltage decay is pronounced, while in the long term it is stabilized at very low self-discharge rates [37]. It is also known that self-discharge is affected by temperature and *SOC*. Temperatures higher than 40 ºC and high *SOC* levels accelerate the self-discharge of LIBs [36], [37].

IV. Experimental Setup

The tests presented below are designed to quantify the degradation of each battery. A non-invasive analysis of the LIBs is proposed for the measurement of capacity, internal resistance, and self-discharge. In all, the study encompassed the four batteries mentioned in Section II-B (E1, E2, E3 and E4) together with two cells that were not taken to Antarctica, referred to as L1 and L2. Cells L1 and L2 have the same characteristics as the batteries used in the expedition but were stored at room temperature at the Energy Storage and Microgrid Laboratory of the Public University of Navarre, safeguarding them from extreme weather conditions. In this way, the aging of E1 – E4 due to extreme weather can be quantified by comparing them to L1 and L2. In order to compare the LIBs analyzed in this study (E1 – E4 4S4P batteries and L1-L2 cells), all the experimental results are presented and treated at cell level.

The methodology consists in performing three charge-discharge cycles at C/3 with voltage limits of 4.2 V and 3 V to obtain the capacity. The charge process was performed by means of the well-known CC-CV protocol with a cut-off current of C/70. Moreover, the last cycle was used to perform an ICA and DV analysis to determine the state of the electrodes and to identify aging phenomena. Further to this, R_{DC} and R_{AC} were measured at each ΔSOC of 20 %. Furthermore, at each *SOC* three EIS measurements were taken in order to ensure repeatability, carefully removing and reinserting the battery/cell. The *SOC* variations were performed at a constant current of C/3, and a 1 h rest period was established before the R_{AC} measurement in order to ensure the electrochemical and thermodynamic stabilization of the LIBs. A schematic representation of the complete test is presented in Fig. 3a.

The R_{DC} was measured through a 10 s current step. Furthermore, the AC internal resistance was measured by imposing a 1 kHz sinusoidal signal on the batteries and recording the real impedance component. The frequency spectra of the EIS range from 50 mHz to 3 kHz. After ensuring repeatability of results, the data were subjected to the linear Kramer Kronig (KK) validity test by means of the free Lin-KK tool [38]. The inductive and diffusion phenomena were then subtracted in order to perform the DRT analysis using the DRT tools [39], a free MATLAB toolbox developed in [40], as represented in the flowchart of Fig. 3b.

The quantification of the self-discharge is done by means of the method described in Section III-C. V_{OC} was periodically measured by means of an ST-9959 multimeter. The first voltage measurements were taken two days after the batteries were charged to a 40 % *SOC*.

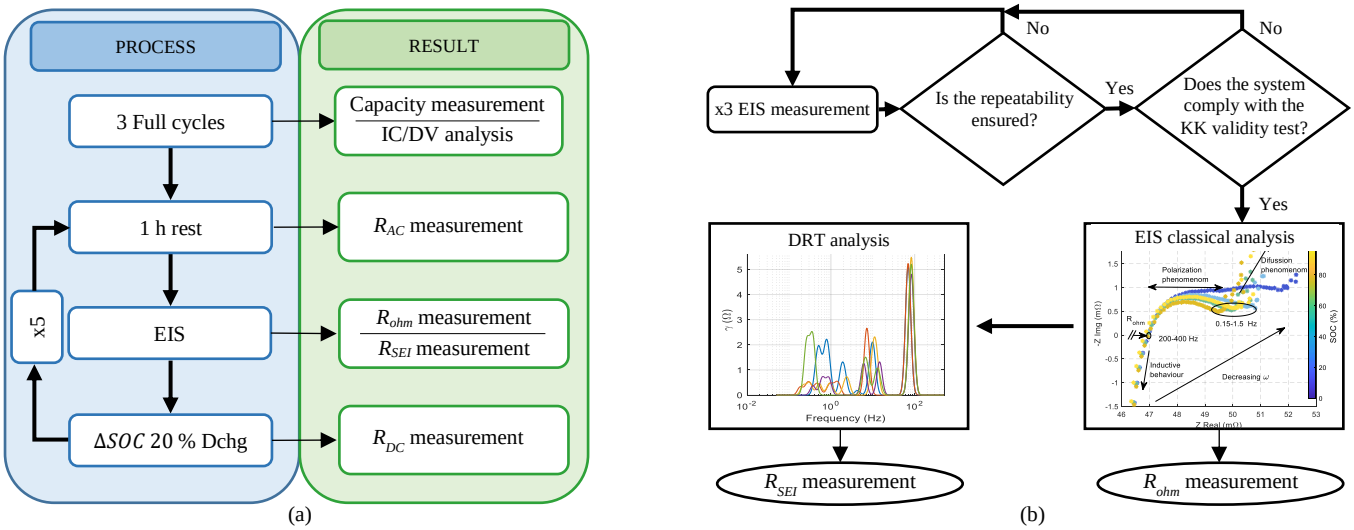

Fig. 3. (a) Schematic representation of the testing protocol. (b) Flowchart of the EIS testing protocol.

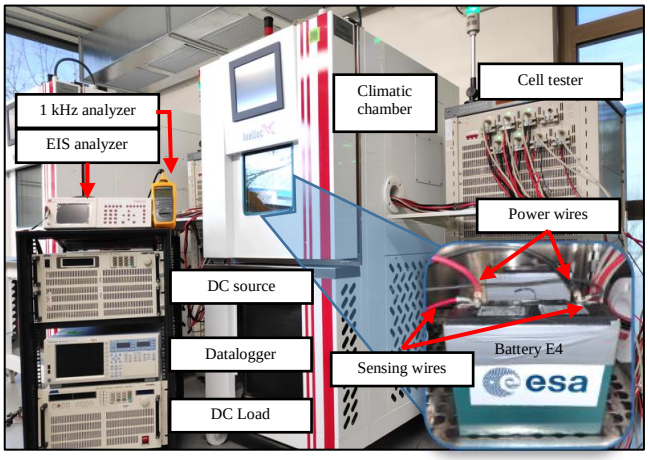

Fig. 4. Picture of test bench located in the Energy Storage and Microgrids Laboratory of the Public University of Navarre.

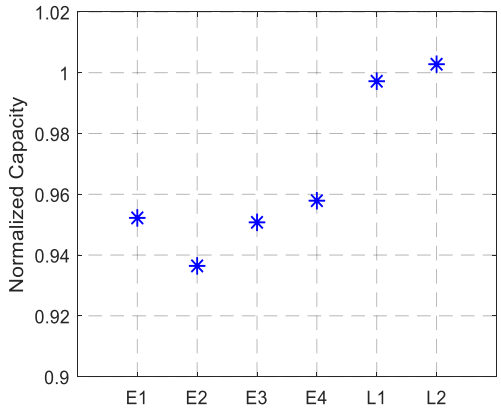

Fig.5. Normalized capacity of each battery.

All the tests and measurements were carried out at the Energy Storage and Microgrid Laboratory of the Public University of Navarre, in an Ineltec INECC-30/300 climatic chamber at a controlled temperature of 25 ºC. All the charge and discharge processes were conducted via an AMREL SPS400X75-K12D source and an AMREL PLA7.5K-600-400 electronic load for E1 – E4, a Neware BTS4000 for L1 and L2, the data acquisition was accomplished by a YOKOGAWA WT1800 Precision Power Analyzer, as shown in Fig. 4. R_{AC} was measured by means of a Fluke BT510 Battery Analyzer. The EIS tests were conducted using a Newtons4th Ltd PSM3750 in tandem with a BATT470m-200 current shunt.

V. Results and Discussion

In this section a comparison is made between the parameters of the batteries deployed during the Antarctic expedition and those of the cells stored in the laboratory, unused and safeguarded from extreme weather conditions. Specifically, the significant factors are capacity, impedance, and self-discharge. Similarly, by means of the capacity measurement in tandem with the ICA/DV analysis and the EIS interpretation using the DRT method, the aging mechanism are identified and indicators linked to hazardous dendrite growth can be detected.

A. Capacity

The measured cell capacities are shown in Fig. 5. For better comparability, these values were normalized to the average capacity of L1 and L2, which are the cells that were not taken on the expedition. This figure shows a capacity fade in the batteries used in the polar expedition of around 5 % compared to the cells kept in the laboratory. This capacity fade is in line with conclusions from previous research studies that identify temperature variations as an LIB aging accelerator [41].

Nevertheless, there is only a slight difference when comparing the capacities of the four batteries used in the expedition, even considering E4, which was not used in the journey. Therefore, capacity fade cannot be merely attributed to cycle aging, and instead seems to be mostly related to calendar aging. E2, which was kept at 100 % *SOC* during the expedition, shows the highest capacity fade. As published in previous research works, high *SOC* levels at temperatures under –20 ºC catalyze the side reactions enhancing LLI, thereby increasing the irreversible capacity fade [37]. E4 and E2, which were not cycled during the expedition, show a difference in capacity fade of 2.2 %. Hence, storing lithium batteries at a high *SOC* (100 %) could lead to accelerated aging.

With regard to cyclability, E1 and E3 were cycled during the expedition less than 50 EFC at a current of less than 0.1 C. The difference in capacity fade between these two cells is minimal, being only 0.15 %. This value is lower than the standard deviation observed in extensive cell testing studies, where values of 0.16 – 0.22 % were reported [36], [42]. Therefore, the cycling profile seems to have a limited effect on aging at low currents and in frigid conditions. The capacity fade difference between the cycled batteries and the one stored at *SOC*=80 % (E4) is 0.57 %, which is negligible.

The reported results lead to the conclusion that calendar aging due to very high *SOC* has a more significant impact on capacity fade than cycling at very low currents in these frigid conditions. Nevertheless, due to the reduced number of samples it is complicated to reach definite conclusions.

In any case, the scope of this work is to propose a non-invasive procedure to characterize battery aging, and asses the safeness of reusing a battery. To this end, the capacity test serves to surmise the current state of the electrodes by virtue of ICA/DV. Fig. 6 shows the ICA and DV of the cells that were taken on, and used in the expedition to Antarctica and the ones stored at a temperature of 25 ºC. Fig. 6a shows the ICA during charge. Two major peaks are observed, hereinafter denoted as P1 and P2, respectively appearing at a voltage of 3.58 V and 3.72 V.

TABLE I
Results of IC and DV

	P1		P2		Q_a	Q_b	Q_c
	IC (Ah/V)	V (V)	IC (Ah/V)	V (V)	(p.u.)	(p.u)	(p.u.)
E1	11.09	3.580	16.44	3.733	0.128	0.532	0.285
E2	10.25	3.582	15.49	3.734	0.131	0.520	0.285
E3	11.13	3.579	16.50	3.729	0.132	0.526	0.286
E4	10.38	3.584	15.94	3.729	0.134	0.536	0.282
L1	11.00	3.574	17.82	3.718	0.135	0.533	0.327
L2	10.95	3.572	18.36	3.716	0.126	0.538	0.337

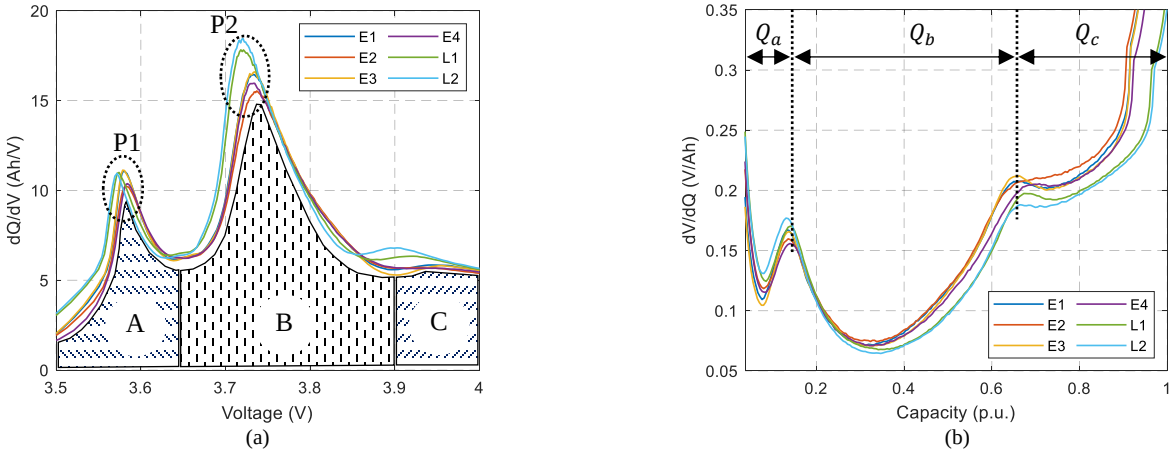

Fig. 6. (a) Results of IC analysis. (b) Results of DV analysis.

As summarized in Table 1 there is a minimal variation in the peak amplitude of P1 among the cells, the maximum difference being 0.75 Ah/V. Although, at first sight, the shape and location of P1 could reveal a correlation with the aging conditions. Fig. 6a shows that E1 and E3 are almost superposed, as well as L1 and L2. Note that E1 and E3 were cycled and L1 and L2 were stored in the laboratory. E2 and E4 are also almost superposed. However, the intensity of P2 is clearly lower in the batteries taken on the expedition. In the case of E2 the intensity of the peak was reduced by 2.87 Ah/V compared to L2, which corresponds to a reduction of 15.6 %. Both peaks were shifted to the right, P1 moved a maximum of 12.3 mV, 17.8 mV in the case of P2. This effect is well reported as being caused by an increase in the internal resistance [12], [14], [20], being in line with the results presented in the following subsections.

Similarly, Fig. 6b shows the absolute value of DV during discharge, for reasons of comparison the capacity has been normalized to the one presenting a maximum value. The widths of Q_a, Q_b and Q_c correspond to areas A, B and C in ICA respectively. Note that, for correct visualization, Fig. 6a has been zoomed and the full voltage spectrum is not visible.

From the results depicted in Table 1, it can be observed that Q_c is lower in the batteries taken on the expedition, with the capacity linked to Q_c having the maximum difference of 5.5 %. Nonetheless, Q_a and Q_b remain virtually invariant, recording a maximum variation of 1 % and 1.9 % respectively. Outwardly, since Q_a and Q_b remain almost constant there is no loss of active material on the anode and the capacity fade can be allegedly related to LLI.

In the case of the cells studied in this paper, no peak growth associated with lithium plating is measured. In fact, P2 decreased by a maximum of 15.6 %, whereas in other studies it dropped to 20 % for a capacity fade of nearly 10 % [14]. Therefore, no risk indicator is observed and assumedly the batteries were aged without a sharp increase in the lithium plating or LLI that could provoke dendrite growth. Nevertheless, it is of great relevance to analyze any possible dendrite growth. With this aim in mind, as detailed in the following subsections, a study on impedance has been conducted. An analysis of R_{SEI} by means of the EIS makes it possible to identify the formation of passive films on the surface of plated lithium [18], an indicator of dendrite growth.

B. *Internal Resistance*

The internal resistance was analyzed using three different techniques: applying a current step to obtain R_{DC}; single-point frequency technique to measure R_{AC} at 1 kHz; and by means of the EIS. A detailed study of the effect that the use of LIBs under extreme cold weather has on the *1)* R_{DC}, *2)* R_{AC} and *3)* R_{ohm} is provided below. Moreover, the underlying aging mechanisms are inferred by means of a DRT analysis, which quantifies the *4)* R_{SEI} increase.

1) R_{DC} *– current steps*: Fig. 7 shows the R_{DC} measured as a function of *SOC*. The 30 % increase in resistance recorded by the batteries used in the expedition is noteworthy, given that it represents a higher degradation rate than the 5% reported in Section V-A based on capacity fade.

2) R_{AC} *– single-point frequency technique*: Fig. 8 shows the values of R_{AC} measured at a frequency of 1 kHz as a function of *SOC*. Even though R_{AC} shows no dependency on *SOC*, it is noteworthy that higher degradation is measured in the batteries with more demanding use (E1 and E3).

3) R_{ohm}: The EIS spectra of all the batteries are illustrated in Fig. 9a for a *SOC* of 80 %. It can be seen that the impedances of the batteries used in the expedition are displaced to the right

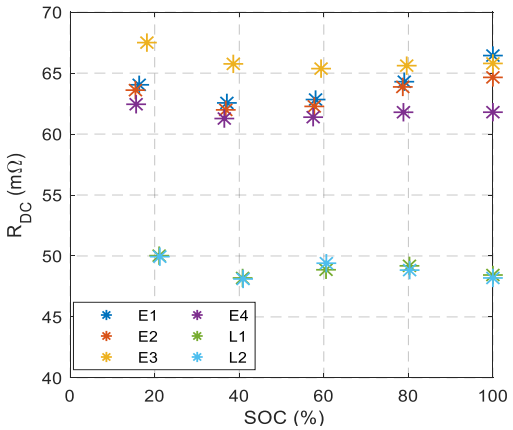

Fig. 7. R_{DC} measurements for different *SOC* values.

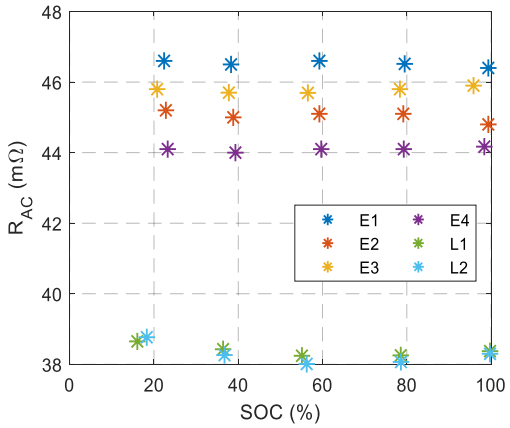

Fig. 8. R_{AC} measurements by means of the single-point frequency technique.

when compared to cells L1 and L2. That means, that the real part of the impedance has risen due to an increase in ohmic resistance. This issue has been reported to be related to the decomposition of the electrolyte and, therefore, to LLI [33]. Low temperatures induce an increase in the viscosity of the electrolyte, reducing its ionic conductivity, and hindering the ionic intercalation in the graphite layers. The metallic lithium plating on the anode surface is highly reactive to the electrolyte, thereby consuming lithium inventory form the electrolyte. The irreversible loss of the electrolyte results in a reduction in ionic conductivity [21], causing an increase in R_{ohm}.

The R_{ohm} of each battery as a function of *SOC* is presented in Fig. 9b. As in the case of R_{AC}, R_{ohm} remains constant between the maximum and minimum *SOC*. There is a substantial difference close to 7.5 mΩ between the ohmic resistance of the LIBs stored in the laboratory and the ones taken on the expedition.

The EIS test permits the study of the frequency that produces an ohmic response of the battery. In this regard, Fig. 9c shows the measured characteristic frequency. From Fig. 9c, it can be observed that frequency decreases with aging, while the impedance increases. The frequency of L1 and L2 ranges between 400 – 450 Hz, whereas the ohmic resistance of the expedition batteries has a frequency range of 200 – 250 Hz.

4) R_{SEI}: The DRT method is used to identify electrochemical phenomena measured by the EIS test. Fig. 10a shows, as an illustrative example, the DRT analysis of L1. Three clear phenomena with different time constants can be identified. The area covered by the blue rectangle, embracing frequencies close to 70 Hz, is attributed to the SEI, as explained in Section III-B. In line with previous literature [30], no significant variations of these phenomena are found for the entire *SOC* range. The red rectangle, with frequencies ranging between 4 and 10 Hz, is attributed to the charge transfer at the anode due to the reduction in the characteristic frequency observed for low *SOC*. Finally, the peaks located in the black rectangle can be attributed to the charge transfer at the NCA cathode. Its frequency ranges from 0.2 to 1.8 Hz, in accordance with previous reports [30].

As reported in the literature, plated lithium on the anode reacts with the electrolyte forming a new SEI film that covers the surface of the plated lithium [21]. SEI impedance is known to be a sum of the thickness, the morphology and the chemical composition of the SEI layer [43]. Hence, a deposition of inactive material on the SEI should be noticeable in the EIS spectra at high frequencies. The phenomenon linked to R_{SEI} is quantified by means of the DRT as the peak value identified at the frequency range of 40 – 70 Hz.

Fig. 10b shows the R_{SEI} values for the six batteries at five *SOC* levels. No significant variation between the LIBs is found, even though E4 presents the lowest impedance and L2 the highest. The lack of an increase in the impedance of the cycled cells denotes that no lithium plating has occurred, and that dendrite growth has been avoided. In fact, the impedance variation between E4, L1 and L2 could be attributed to the storage temperature. Higher temperatures increase SEI layer thickness [44], whereas cycling at freezing temperatures promotes lithium plating and dendrite growth.

In order to assess the safety of LIBs due to dendrite growth, our results were compared to previous studies. Where an increase of almost 2.5 times in the SEI impedance was observed without entailing a risk at high temperatures [31]. Similarly, a study performed at low temperatures reported a variation in the R_{DC} of up to 2 times, following a study of the SEI growth in a post-mortem analysis at a microscopic level in opened cells [21], precluding direct comparison. With regard to the cells

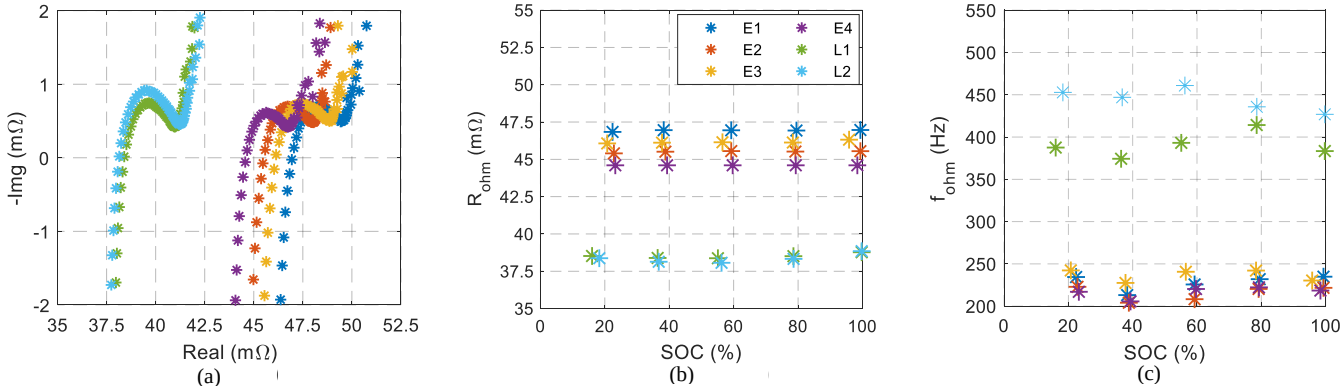

Fig. 9. (a) EIS results for the six batteries for a *SOC* of 80 %. (b) R_{ohm} measurements for different *SOC* values. (c) Characteristic frequency of R_{ohm} for different *SOC* values.

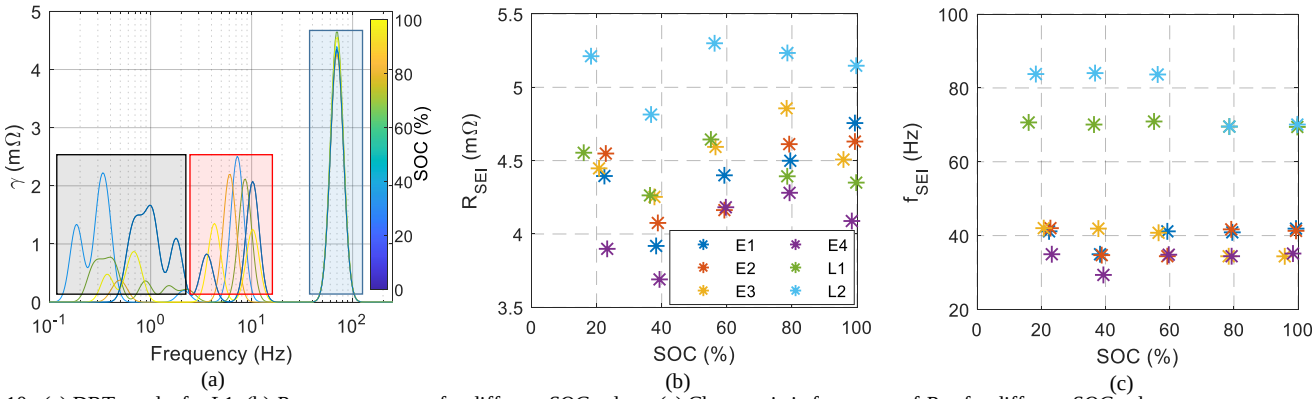

Fig. 10. (a) DRT results for L1. (b) R_{SEI} measurements for different *SOC* values. (c) Characteristic frequency of R_{SEI} for different *SOC* values.

studied in this paper, no increase in the R_{SEI} impedance was observed and the R_{DC} only increased by 30 %. Hence, it can be concluded that no clear indicator of lithium plating causing dendrite growth can be inferred. The results obtained in this subsection are in line with those obtained from the ICA/DV analysis. Therefore, no hazardous indicator can be observed, and seemingly the batteries can be safely used in future expeditions.

Fig. 10c shows the SEI characteristic frequency of the batteries. At first sight, a significant difference in the frequencies between the batteries that were used during the expedition and the ones stored in the laboratory can be seen. With regard to the batteries that were taken on the expedition, E2 and E4, which were hardly used, have similar frequencies, while E1 and E3, which had similar profiles, also present similar frequencies. Typically, degradation models based on EIS have used variations in resistance as an indicator of the aging mechanisms. However, the results shown in this work suggest that variations in the characteristic frequency of R_{ohm} and R_{SEI} could be used for state of health (*SOH*) estimation. Interesting research questions for future investigation can be derived from this observation.

C. Self-discharge

Fig. 11 shows the *SOC* decay of each cell over 13 weeks of storage. From this data, self-discharge can be divided into short-term and long-term. The border between them can be seen to be around 20 days, in line with previous studies [37].

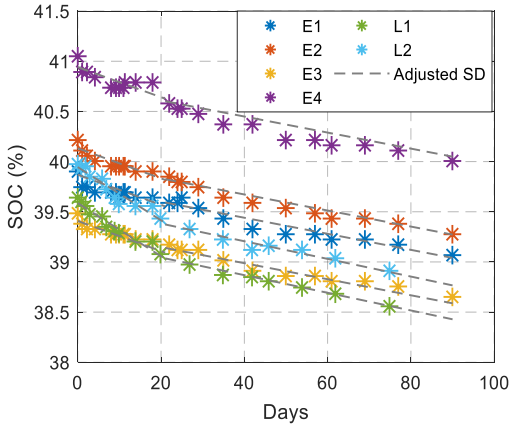

Fig. 11. Self-discharge along days on storage.

The long-term self-discharge of all batteries is virtually the same, with a value of 0.008 % per day. However, the batteries used in the expedition had a lower short-term self-discharge (0.015 % per day) than those stored in the laboratory (0.0265 % per day). For the sake of comparability, a linear dependency of the self-discharge and the storage time has been included in Fig. 11 both for short- and long-term. Dashed lines have slopes of – 0.015 % and – 0.008 % per day for short and long term, respectively for E1 – E4. L1 and L2 lines differ from the previous ones, having slopes of – 0.0265 % per day in the short term and – 0.0088 % per day in the long term.

Due to the reduced amount of data, it is not possible to put forward a justification of the difference in the short-term self-discharge. However, there are two main reasons that could explain this behavior. The first is based on the fact that the self-discharge decreases as the capacity fades. As proposed in a previous publication [45], self-discharge can be expressed in terms of *SOH*, temperature and *SOC*. In our study the cells were stored at the same *SOC* (40 %) and same temperature (25ºC). Thus, the difference can only be explained by the difference in the *SOH*. The second presumption is based on the fact that, during storage at frigid temperatures, the reactions causing calendar aging are slowed down [46]. Given that the side reactions leading to calendar aging are linked to self-discharge, after a long exposure to freezing conditions, the kinetics of the side reactions may have been permanently slowed.

VI. Conclusions

This paper presents a non-invasive analysis of the operation of commercial lithium-ion batteries used in the WindSled Project during a 52-day expedition with temperatures down to – 50 ºC. Hence, the feasibility of using LIBs with an improved electrolyte under extreme frigid conditions with no heating has been demonstrated. The degradation of these batteries during the expedition is characterized in this study. The capacity is reported to fade by 5 % and LLI has been identified as being the main mechanism responsible for this. Furthermore, from the interpretation of the ICA/DV analysis and DRT method, no clear indicator related to lithium plating causing dendrite growth has been detected. These results indicate that the batteries can safely be re-used.

Finally, a 43 % decrease in the self-discharge of the cells taken on the expedition was reported independently of the calendar or cycle aging. The identification of the cause of this self-discharge decrease is highlighted as a relevant area for future investigation.

ACKNOWLEDGMENT

We would like gratefully to acknowledge the members of Antarctica Unexplored Expedition 2018 – 2019, Ramón Larramendi, Ignacio Oficialdegui, Manuel Olivera and Hilo Moreno, for their altruistic collaboration with scientific projects, and for their commitment against climate change.

REFERENCES

[1] E. Martinez-Laserna *et al.*, "Technical Viability of Battery Second Life: A Study from the Ageing Perspective," *IEEE Trans. Ind. Appl.*, vol. 54, no. 3, pp. 2703–2713, 2018, doi: 10.1109/TIA.2018.2801262.

[2] A. Berrueta, M. Heck, M. Jantsch, A. Ursúa, and P. Sanchis, "Combined dynamic programming and region-elimination technique algorithm for optimal sizing and management of lithium-ion batteries for photovoltaic plants," *Appl. Energy*, vol. 228, no. February, pp. 1–11, 2018, doi: 10.1016/j.apenergy.2018.06.060.

[3] R. Youssef *et al.*, "Experimental and numerical study on the thermal behavior of a large lithium-ion prismatic cell with natural air convection.," *IEEE Trans. Ind. Appl.*, vol. 9994, no. c, 2021, doi: 10.1109/TIA.2021.3108757.

[4] E. Schaltz, D. I. Stroe, K. Norregaard, L. S. Ingvardsen, and A. Christensen, "Incremental Capacity Analysis Applied on Electric Vehicles for Battery State-of-Health Estimation," *IEEE Trans. Ind. Appl.*, vol. 57, no. 2, pp. 1810–1817, 2021, doi: 10.1109/TIA.2021.3052454.

[5] A. Berrueta, A. Urtasun, A. Ursúa, and P. Sanchis, "A comprehensive model for lithium-ion batteries: From the physical principles to an electrical model," *Energy*, vol. 144, pp. 286–300, 2018, doi: 10.1016/j.energy.2017.11.154.

[6] A. A. Hussein and A. A. Fardoun, "An Adaptive Sensorless Measurement Technique for Internal Temperature of Li-Ion Batteries Using Impedance Phase Spectroscopy," *IEEE Trans. Ind. Appl.*, vol. 56, no. 3, pp. 3043–3051, 2020, doi: 10.1109/TIA.2020.2979783.

[7] E. Braco, I. San Martin, A. Berrueta, P. Sanchis, and A. Ursua, "Experimental Assessment of First- And Second-Life Electric Vehicle Batteries: Performance, Capacity Dispersion, and Aging," *IEEE Trans. Ind. Appl.*, vol. 57, no. 4, pp. 4107–4117, 2021, doi: 10.1109/TIA.2021.3075180.

[8] X. Wu, Z. Cui, E. Chen, and J. Du, "Capacity degradation minimization oriented optimization for the pulse preheating of lithium-ion batteries under low temperature," *J. Energy Storage*, vol. 31, no. December 2019, p. 101746, 2020, doi: 10.1016/j.est.2020.101746.

[9] A. Soto, A. Berrueta, P. Sanchis, A. Ursua, and I. Oficialdegui, "On the technical reliability of Lithium-ion batteries in a zero emission polar expedition," *Proc. - 2020 IEEE Int. Conf. Environ. Electr. Eng. 2020 IEEE Ind. Commer. Power Syst. Eur. EEEIC / I CPS Eur. 2020*, 2020, doi: 10.1109/EEEIC/ICPSEurope49358.2020.9160601.

[10] SAFT, "MP 176065 xtd Rechargeable Li-ion cell." https://www.saftbatteries.com/products-solutions/products/mp-small-vl (accessed Sep. 22, 2021).

[11] D. Prevot, Y. Borthomieu, E. Ligneel, R. Hague, J. P. Peres, and C. Cenac-Morthe, "Performances of Saft Lithium-Ion Cells in LEO Cycling," *E3S Web Conf.*, vol. 16, no. 1, pp. 1–8, 2017, doi: 10.1051/e3sconf/20171606005.

[12] A. Barai *et al.*, "A comparison of methodologies for the non-invasive characterisation of commercial Li-ion cells," *Prog. Energy Combust. Sci.*, vol. 72, pp. 1–31, 2019, doi: 10.1016/j.pecs.2019.01.001.

[13] A. Soto, A. Berrueta, P. Sanchis, and A. Ursua, "Analysis of the main battery characterization techniques and experimental comparison of commercial 18650 Li-ion cells," *Proc. - 2019 IEEE Int. Conf. Environ. Electr. Eng. 2019 IEEE Ind. Commer. Power Syst. Eur. EEEIC/I CPS Eur. 2019*, pp. 1–6, 2019, doi: 10.1109/EEEIC.2019.8783862.

[14] Y. Li *et al.*, "A quick on-line state of health estimation method for Li-ion battery with incremental capacity curves processed by Gaussian filter," *J. Power Sources*, vol. 373, no. June 2017, pp. 40–53, 2018, doi: 10.1016/j.jpowsour.2017.10.092.

[15] M. Dubarry *et al.*, "Evaluation of commercial lithium-ion cells based on composite positive electrode for plug-in hybrid electric vehicle applications. Part II. Degradation mechanism under 2 C cycle aging," *J. Power Sources*, vol. 196, no. 23, pp. 10336–10343, 2011, doi: 10.1016/j.jpowsour.2011.08.078.

[16] M. Dubarry *et al.*, "Evaluation of commercial lithium-ion cells based on composite positive electrode for plug-in hybrid electric vehicle applications. Part I: Initial characterizations," *J. Power Sources*, vol. 196, no. 23, pp. 10328–10335, 2011, doi: 10.1016/j.jpowsour.2011.08.077.

[17] P. Keil *et al.*, "Calendar Aging of Lithium-Ion Batteries," *J. Electrochem. Soc.*, vol. 163, no. 9, pp. A1872–A1880, 2016, doi: 10.1149/2.0411609jes.

[18] Y. Tian, C. Lin, H. Li, J. Du, and R. Xiong, "Detecting undesired lithium plating on anodes for lithium-ion batteries – A review on the in-situ methods," *Appl. Energy*, vol. 300, no. February, p. 117386, 2021, doi: 10.1016/j.apenergy.2021.117386.

[19] C. Pastor-Fernández, K. Uddin, G. H. Chouchelamane, W. D. Widanage, and J. Marco, "A Comparison between Electrochemical Impedance Spectroscopy and Incremental Capacity-Differential Voltage as Li-ion Diagnostic Techniques to Identify and Quantify the Effects of Degradation Modes within Battery Management Systems," *J. Power Sources*, vol. 360, pp. 301–318, 2017, doi: 10.1016/j.jpowsour.2017.03.042.

[20] D. Ansean *et al.*, "Lithium-Ion Battery Degradation Indicators Via Incremental Capacity Analysis," *IEEE Trans. Ind. Appl.*, vol. 55, no. 3, pp. 2992–3002, 2019, doi: 10.1109/TIA.2019.2891213.

[21] G. Zhang *et al.*, "Lithium plating on the anode for lithium-ion batteries during long-term low temperature cycling," *J. Power Sources*, vol. 484, no. December 2020, p. 229312, 2021, doi: 10.1016/j.jpowsour.2020.229312.

[22] D. Anseán *et al.*, "Operando lithium plating quantification and early detection of a commercial LiFePO4 cell cycled under dynamic driving schedule," *J. Power Sources*, vol. 356, pp. 36–46, 2017, doi: 10.1016/j.jpowsour.2017.04.072.

[23] M. Dubarry, M. Berecibar, A. Devie, D. Anseán, N. Omar, and I. Villarreal, "State of health battery estimator enabling degradation diagnosis: Model and algorithm description," *J. Power Sources*, vol. 360, pp. 59–69, 2017, doi: 10.1016/j.jpowsour.2017.05.121.

[24] E. Braco, I. San Martín, A. Berrueta, P. Sanchis, and A. Ursúa, "Experimental assessment of cycling ageing of lithium-ion second-life batteries from electric vehicles," *J. Energy Storage*, vol. 32, no. May, p. 101695, 2020, doi: 10.1016/j.est.2020.101695.

[25] A. Soto, A. Berrueta, P. Sanchis, and A. Ursua, "Influence of renewable power fluctuations on the lifetime prediction of lithium-ion batteries in a microgrid environment," *Proc. - 2019 IEEE Int. Conf. Environ. Electr. Eng. 2019 IEEE Ind. Commer. Power Syst. Eur. EEEIC/I CPS Eur. 2019*, 2019, doi: 10.1109/EEEIC.2019.8783260.

[26] Y. Zhang, Q. Tang, Y. Zhang, J. Wang, U. Stimming, and A. A. Lee, "Identifying degradation patterns of lithium ion batteries from impedance spectroscopy using machine learning," *Nat. Commun.*, vol. 11, no. 1, pp. 6–11, 2020, doi: 10.1038/s41467-020-15235-7.

[27] N. Meddings *et al.*, "Application of electrochemical impedance spectroscopy to commercial Li-ion cells: A review," *J. Power Sources*, vol. 480, no. July, 2020, doi: 10.1016/j.jpowsour.2020.228742.

[28] C. Fleischer, W. Waag, H. M. Heyn, and D. U. Sauer, "On-line adaptive battery impedance parameter and state estimation considering physical principles in reduced order equivalent circuit battery models: Part 1. Requirements, critical review of methods and modeling," *J. Power Sources*, vol. 260, pp. 276–291, 2014, doi: 10.1016/j.jpowsour.2014.01.129.

[29] F. Hall, J. Touzri, S. Wußler, H. Buqa, and W. G. Bessler, "Experimental investigation of the thermal and cycling behavior of a lithium titanate-based lithium-ion pouch cell," *J. Energy Storage*, vol. 17, pp. 109–117, 2018, doi: 10.1016/j.est.2018.02.012.

[30] P. Shafiei Sabet, G. Stahl, and D. U. Sauer, "Non-invasive investigation of predominant processes in the impedance spectra of high energy lithium-ion batteries with nickel–cobalt–aluminum cathodes," *J. Power Sources*, vol. 472, no. July, p. 228189, 2020, doi: 10.1016/j.jpowsour.2020.228189.

[31] P. Shafiei Sabet, A. J. Warnecke, F. Meier, H. Witzenhausen, E. Martinez-Laserna, and D. U. Sauer, "Non-invasive yet separate investigation of anode/cathode degradation of lithium-ion batteries (nickel–cobalt–manganese vs. graphite) due to accelerated aging," *J. Power Sources*, vol. 449, no. October 2019, p. 227369, 2020, doi: 10.1016/j.jpowsour.2019.227369.

[32] B. Manikandan, V. Ramar, C. Yap, and P. Balaya, "Investigation of phys-

ico-chemical processes in lithium-ion batteries by deconvolution of electrochemical impedance spectra," *J. Power Sources*, vol. 361, pp. 300–309, 2017, doi: 10.1016/j.jpowsour.2017.07.006.
[33] X. Zhou, Z. Pan, X. Han, L. Lu, and M. Ouyang, "An easy-to-implement multi-point impedance technique for monitoring aging of lithium ion batteries," *J. Power Sources*, vol. 417, no. November 2018, pp. 188–192, 2019, doi: 10.1016/j.jpowsour.2018.11.087.
[34] P. Shafiei Sabet and D. U. Sauer, "Separation of predominant processes in electrochemical impedance spectra of lithium-ion batteries with nickel–manganese–cobalt cathodes," *J. Power Sources*, vol. 425, no. March, pp. 121–129, 2019, doi: 10.1016/j.jpowsour.2019.03.068.
[35] T. P. Heins, N. Schlüter, and U. Schröder, "Electrode-Resolved Monitoring of the Ageing of Large-Scale Lithium-Ion Cells by using Electrochemical Impedance Spectroscopy," *ChemElectroChem*, vol. 4, no. 11, pp. 2921–2927, 2017, doi: 10.1002/celc.201700686.
[36] I. Zilberman, S. Ludwig, and A. Jossen, "Cell-to-cell variation of calendar aging and reversible self-discharge in 18650 nickel-rich, silicon–graphite lithium-ion cells," *J. Energy Storage*, vol. 26, no. June, p. 100900, 2019, doi: 10.1016/j.est.2019.100900.
[37] T. Deutschen, S. Gasser, M. Schaller, and J. Siehr, "Modeling the self-discharge by voltage decay of a NMC/graphite lithium-ion cell," *J. Energy Storage*, vol. 19, no. June, pp. 113–119, 2018, doi: 10.1016/j.est.2018.07.003.
[38] "Lin-KK tool." http://www.iam.kit.edu/wet/Lin-KK.php.
[39] "DRTtools." sites.google.com/site/drttools/.
[40] T. H. Wan, M. Saccoccio, C. Chen, and F. Ciucci, "Influence of the Discretization Methods on the Distribution of Relaxation Times Deconvolution: Implementing Radial Basis Functions with DRTtools," *Electrochim. Acta*, vol. 184, pp. 483–499, 2015, doi: 10.1016/j.electacta.2015.09.097.
[41] W. Chang, C. Bommier, T. Fair, J. Yeung, S. Patil, and D. Steingart, "Understanding Adverse Effects of Temperature Shifts on Li-Ion Batteries: An Operando Acoustic Study," *J. Electrochem. Soc.*, vol. 167, no. 9, p. 090503, 2020, doi: 10.1149/1945-7111/ab6c56.
[42] C. Campestrini, P. Keil, S. F. Schuster, and A. Jossen, "Ageing of lithium-ion battery modules with dissipative balancing compared with single-cell ageing," *J. Energy Storage*, vol. 6, pp. 142–152, 2016, doi: 10.1016/j.est.2016.03.004.
[43] P. Lu, C. Li, E. W. Schneider, and S. J. Harris, "Chemistry, impedance, and morphology evolution in solid electrolyte interphase films during formation in lithium ion batteries," *J. Phys. Chem. C*, vol. 118, no. 2, pp. 896–903, 2014, doi: 10.1021/jp4111019.
[44] T. Waldmann, M. Wilka, M. Kasper, M. Fleischhammer, and M. Wohlfahrt-Mehrens, "Temperature dependent ageing mechanisms in Lithium-ion batteries - A Post-Mortem study," *J. Power Sources*, vol. 262, pp. 129–135, 2014, doi: 10.1016/j.jpowsour.2014.03.112.
[45] E. Redondo-Iglesias, P. Venet, and S. Pelissier, "Global model for self-discharge and capacity fade in lithium-ion batteries based on the generalized eyring relationship," *IEEE Trans. Veh. Technol.*, vol. 67, no. 1, pp. 104–113, 2018, doi: 10.1109/TVT.2017.2751218.
[46] M. Dubarry, N. Qin, and P. Brooker, "Calendar aging of commercial Li-ion cells of different chemistries – A review," *Curr. Opin. Electrochem.*, vol. 9, pp. 106–113, 2018, doi: 10.1016/j.coelec.2018.05.023.

Adrian Soto (Student Member, IEEE) received the B.Sc. degree in industrial electronic engineering and automatics from the University of the Basque Country, Leioa, Spain, in 2017, and the M.Sc. degree in renewable energies: electric generation from the Public University of Navarre, Pamplona, Spain, in 2018, where he is currently working toward the Ph.D. degree in electrical engineering with the Power Electronics and Renewable Energy Research Group (INGEPER).

In 2018, he joined INGEPER, where he is currently a Researcher. He has also altruistically collaborated as a Technical Assistant in the WindSled Project. His research interests include renewable energy systems, electric energy storage technologies, lithium-ion batteries, power electronics, energy management, and electric microgrids.

Alberto Berrueta (M'18) received the M.Sc. (Hons.) and Ph.D. degrees in electrical engineering from the Public University of Navarre (UPNA), Spain, in 2013 and 2017, respectively.

In 2013, he joined the Electrical Engineering, Power Electronics and Renewable Energy Research Group (Ingeper) at UPNA, where he is currently an Assistant Professor and a Linked Researcher at the Research Institute of Smart Cities. His research interests include electrochemical modeling, aging and energy management algorithms for lithium-ion batteries.

Ignacio Oficialdegui received B.Sc. in Biology at the University of Navarre (UN), Spain, in 1990. In 1993, he obtained a Master degree in Environmental Impact Assessment from Universidad Complutense de Madrid, Spain, and in Environmental Management from the University of Malaga, Spain.In 2013, he obtained an MBA in Sustainable Economy from Industrial Organization School in Madrid.

In 1993-1997, he worked in International Development Cooperation in Croatia, Zimbabwe and Rwanda. In 1997, he joined Energía Hidroeléctrica de Navarra, that latter became Acciona Energy company, where he is today the Director of Wind and PV Technology. With his company, he has been developing Renewable Energy projects in more than 70 countries and founded technical teams in 21 of them.

In 2000, he started his career as Polar Explorer, using uniquely Wind and Sun as energy source. He has crossed 3 times Antarctica and 1 Greenland in Extreme scientific expeditions in collaboration with 16 Scientific organizations.

In 2020, he was admitted as Member of the Explorers Club of New York.

Pablo Sanchis (M'03-SM'12) received the M.Sc. degree in electrical engineering, the M.Sc. degree in management and business administration, and the Ph.D. degree in electrical engineering from the Public University of Navarre (UPNA), Pamplona, Spain, in 1994, 1995, and 2002, respectively.

From 1996 to 1998, he was a Guest Researcher with the Delft University of Technology, The Nether-

lands. In 1998, he joined the Department of Electrical, Electronic and Communications Engineering, Public University of Navarre, where he is now a Full Professor. He is the Head of both the UPNA Chair for Renewable Energies and the Research Group in Electrical Engineering, Power Electronics, and Renewable Energies. He has been involved in more than 110 research projects both with public funding and in cooperation with industry and is the co-inventor of 14 patents. He has supervised 11 Ph.D. theses and coauthored 160 articles and contributions in international journals and conferences as well as five book chapters (h-index of 35). His current research interests include renewable energies, power electronics, electric energy storage, electric vehicles and hydrogen technologies.
Dr. Sanchis received the UPNA Research Award for the Best Technical Paper in 2013 and the UPNA Excellence in Teaching Award in 2017

Alfredo Ursúa (M'04-SM'20) received B.Sc. and M.Sc. degrees, both with honors, in Electrical Engineering at the Public University of Navarre (UPNA), Spain, in 2001 and 2004, respectively. In 2010, he obtained a Ph.D. in Industrial Engineering from UPNA, and received the Extraordinary Doctoral Award in the field of Telecommunication Technologies, Bioengineering and Renewable Energies.
In 2002, he joined the Department of Electrical, Electronic and Communications Engineering where he is currently Associate Professor. He also belongs to the Electrical Engineering, Power Electronics and Renewable Energy Research Group of the UPNA Institute of Smart Cities (ISC). He is currently the Vice Dean of the School of Industrial & ICT Engineering and a member of the Steering Committee of the University Chair for Renewable Energies. He has been involved in more than 65 research projects both with public funding and in cooperation with industry and is the co-inventor of seven patents. He has supervised three Ph.D. thesis and coauthored more than 85 papers and contributions in international journals and conferences as well as three book chapters. In 2013, he received the UPNA Research Award for the Best Technical Paper. His research interests include renewable energy systems, electric energy storage technologies, power electronics, energy management and electric microgrids.